and (8) should agree with each other in the limit when r approaches unity, the following result is obtained:

$$C(\theta) = \pi\sqrt{b/a}(a^2 \cos^2\theta + b^2 \sin^2\theta)^{1/4}A(\theta)/\cos\theta \quad (9)$$

Once the function $C(\theta)$ has been determined, the sectional suction force coefficient becomes

$$c_s = -\pi^3\sqrt{\cos^2\theta + k^2 \sin^2\theta}A^2(\theta)/2 \cos^3\theta \quad (10)$$

and the total suction force coefficient is

$$C_S = -2\pi^2 \int_{\pi/2}^{\pi} \frac{\sqrt{\cos^2\theta + k^2 \sin^2\theta}A^2(\theta)}{\cos\theta} \, d\theta \quad (11)$$

Hence, the sectional induced drag coefficient is given by $c_{di}^N = c_l\alpha - c_s$, and the total induced drag coefficient by $C_{Di}^N = C_L\alpha - C_S$. The suffix N denotes the near field, c_l is the sectional lift coefficient, C_L is the total lift coefficient, and α is the angle of attack. The definite integral in Eq. (11) is evaluated numerically, and the lift coefficients are calculated from Eq. (3).

Numerical Results

In numerical examples α is assumed to be 1 rad. Table 1 shows a comparison study of the total induced drag between the present method and two kinds of lifting-line theories.[8] Two lifting-line theories are unable to predict the near-field induced drag. This result confirms the validity of the present analysis because the agreement of two kinds of induced drags is good. Figures 2a and 2b show the spanwise distributions of the sectional induced drags by the present analysis for the cases of Table 1. The sectional distributions of two methods are different near the wingtip of even the large aspect ratio elliptic wing.

Figure 3 shows a comparison result of the total suction force for various values of k. Even the extended lifting-line theory will not estimate induced drag sufficiently at the values of k above about 0.25, that is, of an aspect ratio below about 6.4.

Conclusions

This Note has presented analytical solutions for two kinds of induced drag calculations describing circular and elliptic wings in linearized incompressible steady flow using Kida's method. Good agreement between two kinds of induced drags shows the validity of the present analysis. Moreover, it is shown that the sectional distributions of two kinds of induced drags are different in the case of even the large aspect ratio elliptic wing. Those solutions will be useful in the examination of numerical lifting-surface theories.

References

[1]Kalman, T. P., Giesing, J. P., and Rodden, W. P., "Spanwise Distribution of Induced Drag in Subsonic Flow by the Vortex Lattice Method," *Journal of Aircraft*, Vol. 7, No. 2, 1970, pp. 574–576.

[2]Lan, C. E., "A Quasi-Vortex-Lattice Method in Thin Wing Theory," *Journal of Aircraft*, Vol. 11, No. 9, 1974, pp. 518–527.

[3]Wagner, S., "On the Singularity Method of Subsonic Lifting-Surface Theory," *Journal of Aircraft*, Vol. 6, No. 6, 1969, pp. 549–558.

[4]Medan, R. T., "Improvements to the Kernel Function Method of Steady Subsonic Lifting Surface Theory," NASA TM X-62, 327, March 1974.

[5]Kida, T., "A Theoretical Treatment of Lifting Surface Theory of an Elliptic Wing," *ZAMM*, Vol. 60, 1980, pp. 645–651.

[6]Katz, J., and Plotkin, A., *Low-Speed Aerodynamics: From Wing Theory to Panel Methods*, McGraw–Hill, New York, 1991, Chap. 8.

[7]Robinson, A., and Laurmann, J. A., *Wing Theory*, Cambridge Univ. Press, London, 1956, Chap. 3.

[8]Schlichting, H., and Truckenbrodt, E., *Aerodynamic of the Airplane*, McGraw–Hill, New York, 1979, Chap. 3.

Determination of Aircraft Stall Margins During Takeoff

Sergey Kofman* and Georges A. Bécus†
University of Cincinnati, Cincinnati, Ohio 45221-0070

Nomenclature

C_D = coefficient of drag
C_L = coefficient of lift
$C_{L\max}$ = lift coefficient corresponding to stall angle of attack
$C_{L\text{peak}}$ = lift coefficient corresponding to peak angle of attack
C_m = coefficient of pitching moment
$\bar{c}$ = mean aerodynamic chord, m
D = drag force, N
f = coefficient of friction
H = altitude, m
I_{yy} = Y-body axis moment of inertia, kg-m^2
L = lift force, N
M = aircraft total moment, N-m
M_a = aircraft aerodynamic moment, N-m
M_g = moment generated by landing gears, N-m
m = aircraft mass, kg
Q = pitch rate, rad/s
$\bar{q}$ = dynamic pressure, N/m^2
R_g = normal reaction on the landing gears, N
S = wing planform area, m^2
T = thrust force, N
V = calibrated airspeed, m/s
V_S = calibrated stalling speed, m/s
W = aircraft weight, N
x_{cg} = center of gravity
x_{ac} = aerodynamic center
α = angle of attack, rad
α_{peak} = maximum angle of attack, reached during the maneuver, rad
α_{stall} = stall angle of attack, rad
γ = flight-path angle, rad
δ_{el} = elevator deflection, rad
$\delta_{l.e.}$ = leading-edge device deflection, rad
θ = pitch angle, rad
φ_{eng} = thrust vector angle, rad

Introduction

THE problem of change in aircraft performance because of different configurations (malfunctioning of the control system can leave trailing-edge flaps or leading-edge devices in an inadequate position), as well as various flight conditions, receives considerable theoretical and practical attention during aircraft design, flight tests, and certification. The evaluation of variations in stall characteristics and overall aircraft performance because of an inadequate takeoff configuration is important from a safety standpoint. In the past, several accidents (Northwest DC-9, Detroit[1] and Delta B-727, Dallas[2]) have been associated with an improperly set takeoff configuration (inadvertent flaps-up).

Existing Federal Aviation Regulations (FAR)[3] define stall speed V_S as a calibrated stalling speed or the minimum steady flight speed, in knots, at which the aircraft is controllable, with several conditions, specified in FAR §25.103. Stall margin can

Received March 5, 1995; revision received Oct. 12, 1995; accepted for publication Oct. 17, 1995.

*Graduate Student, Aerospace Engineering and Engineering Mechanics. Student Member AIAA.

†Associate Professor, Aerospace Engineering and Engineering Mechanics. Senior Member AIAA.

be defined based on airspeed or based on lift coefficient. The FAA Advisory Circular (AC) 25-7 (Ref. 4) provides guidelines for the flight test evaluation of transport category aircraft, including stall testing. The configuration stall speeds should be determined for all aerodynamic configurations for use in takeoff, en route, approach, and landing.[3]

Aircraft takeoff configuration (leading-edge device and flaps positions) is predetermined as a result of design, wind-tunnel, and developmental flight tests. The certification flight tests are conducted for this configuration to establish the aircraft takeoff characteristics to be in compliance with FAR. If a failure of the leading-edge device control system (inadvertent retraction of leading edge) occurs at an airspeed $V \geq V_1$ (decision speed), the pilot is committed to takeoff with flaps in the takeoff configuration and retracted leading edge. Determining how the leading-edge device with a combination of various takeoff procedures affects stall margin was the goal of the research reported here.

This determination was carried out using a computer simulation for the takeoff phase of flight utilizing an aircraft model presented in the next section. Some details on the simulation appear in the following section, followed by a section providing typical results of the simulation. Concluding remarks appear at the end of this Note.

Aircraft Model

The computer simulation is based on the mathematical modeling of aircraft motion during the takeoff stage with different rotation rates, pitch angles to be reached by the aircraft after rotation, and rotation speeds. The aerodynamic data for the Tu-154 triple-engine turbojet (similar to B-727)[5] have been used in this simulation.

For the simulation the following assumptions were made: 1) the aircraft is a rigid body, 2) only longitudinal motion is considered, 3) all control surface deflections occur instantaneously, 4) the drag force from control surface deflections is neglected, 5) the aircraft rotates around its c.g. prior to and after liftoff, and 6) the position of engine control levers is not changed during takeoff.

The following equations of aircraft longitudinal motion were used[6,7]:

$$\dot{V} = (1/m)[T\cos(\alpha + \varphi_{\text{eng}}) - W\sin\gamma - D - fR_g] \quad (1)$$

$$\dot{\alpha} = \dot{\theta} - \dot{\gamma} \quad (2)$$

$$\dot{\theta} = Q \quad (3)$$

$$\dot{Q} = M/I_{yy} \quad (4)$$

$$\dot{H} = V\sin\gamma \quad (5)$$

$$\dot{\gamma} = (1/mV)[T\sin(\alpha + \varphi_{\text{eng}}) + C_L\bar{q}S - W\cos\gamma] \quad (6)$$

where

$$L = C_L\bar{q}S$$

$$D = C_D\bar{q}S$$

$$W = mg$$

$$M = M_a - M_g$$

$$C_m = C_{m_0} + C_{m_\alpha}\alpha + C_L(x_{\text{cg}} - x_{\text{ac}}) + C_{m_{\delta\text{el}}}\delta_{\text{el}} + C_{m_{\delta\text{l.e.}}}\delta_{\text{l.e.}}$$

$$M_a = C_m\bar{q}S\bar{c} + (C_{mq}Q + C_{m\dot{\alpha}}\dot{\alpha})(\bar{q}S\bar{c}^2/2V)$$

$$M_g = R_g(x_g - x_{\text{cg}})$$

$$R_g = W - L - T\sin(\alpha + \varphi_{\text{eng}})$$

Simulation Implementation

In the simulation the equations of aircraft motion presented previously are integrated. During this integration the peak angle of attack α_{peak} (i.e., the maximum angle of attack reached by the aircraft during the maneuver) is determined. The lift coefficients corresponding to α_{peak} and α_{stall} are obtained from experimental data $C_L = f(\alpha)$ generated during wind-tunnel testing[5] (see Fig. 1). The simulation is carried out for different aircraft configurations (retracted/extended leading-edge devices), trailing-edge flaps set in the takeoff position, various rotation speeds and rates, and different target pitch angles. The aircraft weight (90% of maximum takeoff weight) and aft c.g. location remain the same throughout the integration for all cases.

The integration of aircraft motion starts from $V = 0$, $\alpha = \alpha_0 = 3$ deg, and $\gamma = 0$ deg when the aircraft is on the runway. When the rotation speed V_R is reached, the elevator is deflected at $\delta_{\text{el}} = -15$ deg. As soon as the total moment M on the aircraft becomes positive, the aircraft starts to rotate about its c.g. and the differential Eq. (4) is integrated from that time on. When Q_{target} is reached, $\dot{Q}$ is set to 0, and Q remains at Q_{target}. When θ [obtained from Eq. (3)] reaches θ_{target}, Q is set to 0 and θ remains at θ_{target}. As soon as the normal reaction R_g of the ground on the landing gears is 0, the aircraft becomes airborne and the integration of γ [Eq. (6)] begins. During the simulation, α_{peak} and $C_{L\text{peak}}$ are determined and the stall margin is calculated.

All of the aerodynamic and moment coefficients used in this simulation were obtained from aircraft experimental data for different positions of leading-edge device and trailing-edge flaps set in the takeoff position. No approximate expression (such as $C_D = C_{D0} + AC_L^2$) for the data was used because of the inaccuracy of such formulas in the nonlinear region of $C_L = f(\alpha)$. Values at intermediate points were linearly interpolated from the aircraft aerodynamic data.

Results

The simulation was carried out for several rotation rates. Typical results obtained for rotation rates $Q = 2$ deg/s and 3 deg/s are presented in Figs. 2–5.

In Figs. 2 and 3 the peak angle of attack and stall margin (in terms of C_L) are presented for $Q = 2$ deg/s. The nominal value of the rotation speed is $V_R = 70$ m/s (≈140 kn). Deviation of ±5 m/s (≈10 kn) from nominal rotation speed was also considered. This range of deviations is considered to be wide enough to account for pilot errors.

As seen on these plots, the position of the leading-edge device during takeoff significantly affects the aerodynamics of the wing and stall margin. On average, retraction of the leading-edge device decreases the stall margin (in terms of C_L)

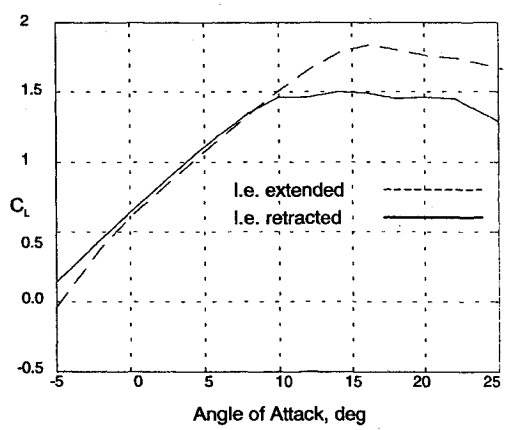

Fig. 1 C_L vs α for extended and retracted leading-edge device. $\delta_{\text{FLAPS}} = 28$ deg (takeoff).

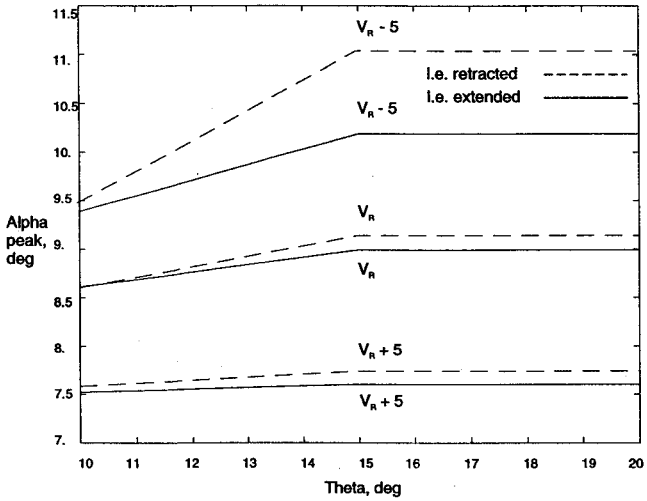

Fig. 2 Peak angle of attack vs pitch angle. Q = 2 deg/s.

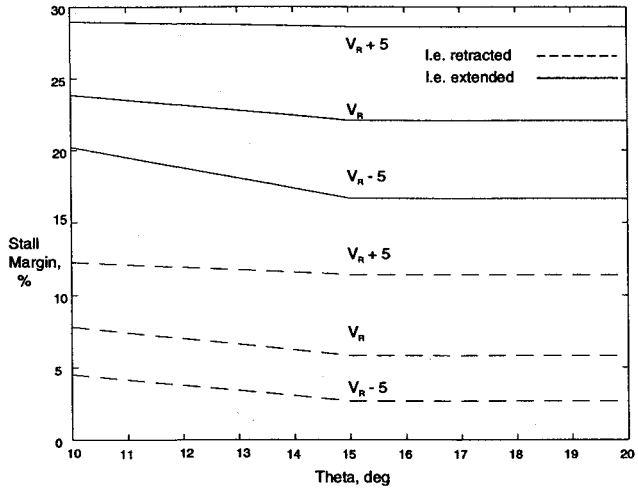

Fig. 3 Stall margin vs pitch angle. Q = 2 deg/s.

by approximately 16%. The corresponding minimum airspeed drops from 1.12 to $1.02V_S$ [where the stall speed $V_S = 1.275\sqrt{W/(SC_{L\max})}$]. At this rotation rate, the safety margin never goes below 0 (i.e., aircraft never stalls) in the range of variations for V_R and θ, although the 3% stall margin and $V_{\min} = 1.02V_S$ obtained in the computer simulation are not sufficient to guarantee that the actual aircraft would always have a positive stall margin as well.

The inflection point on the plots is because, in the simulation, as soon as θ exceeds θ_{target}, Q is instantaneously set to zero. This would not occur in a real aircraft.

The results obtained for rotation rate Q = 3 deg/s and presented in Figs. 4 and 5 are similar. The amount of safety margin (in terms of C_L) lost as a result of the leading-edge device retraction varies from 16% at θ_{target} = 10 deg to 11% for θ_{target} = 20 deg.

If a failure of the leading-edge device control system occurs at an airspeed $V \geq V_1$ so that the pilot is committed to continue takeoff, the problem of maintaining the required rotation speed becomes critical. As seen in Figs. 3 and 5, if the aircraft is rotated at the rotation speed $V_R - 5$ m/s ($\approx V_R - 10$ kn) with pitch rate Q = 2 deg/s, the stall margin is less than 5%, whereas with Q = 3 deg/s the stall margin becomes zero at $\theta \approx 18$ deg, and the aircraft stalls for $\theta > 18$ deg.

Notice also that stall margin is more sensitive to V_R variations for an aircraft with an extended leading-edge device, although the worst case considered with extended leading-edge device ($V_R - 5$ m/s, Q = 3 deg/s) provides a safety margin not less than 7% at the maximum θ considered (20 deg).

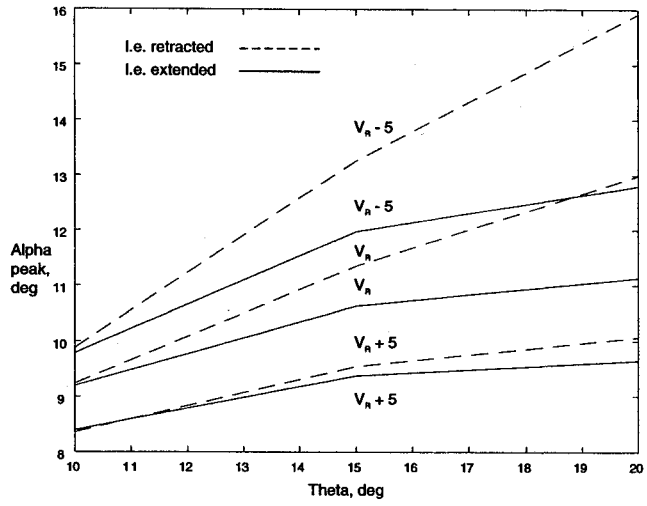

Fig. 4 Peak angle of attack vs pitch attitude. Q = 3 deg/s.

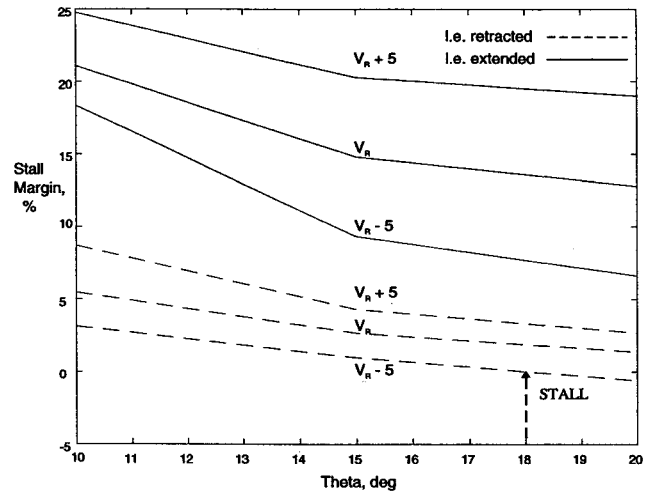

Fig. 5 Stall margin vs pitch angle. Q = 3 deg/s.

The target pitch attitude with extended trailing-edge flaps and leading-edge flaps provides a C_L sufficient for the aircraft to fly, although for high pitch attitude, the airspeed appears less than the required minimum takeoff safety speed $V_{2\min}$. If the leading-edge device is retracted for any reason, the high target pitch attitude does not give enough C_L for the aircraft to fly even with extended trailing-edge flaps in the takeoff position. The lower pitch attitude gives a positive safety margin, but the value yielded by the simplified model of this study is too small to guarantee that the actual aircraft has sufficient C_L to avoid stall.

Conclusions

For the Tu-154 aircraft inadvertent retraction of leading-edge devices significantly affects stall margin. This, in combination with nonaccurate maintaining of the required rotation speed and/or excessive rotation rate, may lead to aircraft stall. If such a failure is not considered as extremely improbable ($P > 10^{-9}$), recommended actions to the crew in the event of such failure should be included in the Flight Manual. All results presented here are based on a computer simulation (which involves several simplifying assumptions); they would require confirmation in test flights to ensure that they are accurate enough to be used in generating recommendations for the Aircraft Flight Manual.

Acknowledgments

The work of the first author was supported in part by the Naticnal Transportation Safety Board under Research Grant RA-3-013 to the second author.

References

[1]Aircraft Accident Report—Northwest Airlines, Inc., McDonnell Douglas DC-9-82, N312RC, Detroit Metropolitan Wayne County Airport, Romulus, MI, Aug. 16, 1987; National Transportation Safety Board, 1988.

[2]Aircraft Accident Report—Delta Air Lines, Inc., Boeing 727-232, N473DA, Dallas–Fort Worth International Airport, TX, Aug. 31, 1988; National Transportation Safety Board, 1989.

[3]Airworthiness Standards: Transport Category Airplanes, 14CFR Pt. 25, Jan. 1994, Paragraph 25.103.

[4]Flight Test Guide for Certification of Transport Category Aircraft, U.S. Dept. of Transportation, FAA, Advisory Circular 25-7, 1986.

[5]Ligum, S. U., Scripnichenko, L. A., Chulsky, A. V., Shishmareyv, S. I., and Yurovsky, S. I., *Aerodinamica Samoleta Tu-154*, Transport, Moscow, 1977.

[6]Stevens, B. L., and Lewis, F. L., *Aircraft Control and Simulation*, Wiley, New York, 1992.

[7]Nelson, R. C., *Flight Stability and Automatic Control*, McGraw–Hill, New York, 1989.

Approximate Formula for the Frequencies of a Rotating Timoshenko Beam

V. T. Nagaraj*
Hindustan Aeronautics Ltd.,
Bangalore 560017, India

Introduction

It is well known that shear deformation and rotary inertia can have an important influence on the frequencies of nonrotating beams. This influence can be especially significant for beams made of advanced composite materials because of the high ratio of Young's modulus to the shear modulus. For nonrotating beams, these effects can be modeled by Timoshenko's equations for which exact solutions are available.[1,2]

An approximate formula for the frequencies and mode shapes of rotating uniform cantilever Euler–Bernoulli beams is given by Peters.[3] The expression given by Peters is simple and very accurate for the entire blade stiffness range. It gives accurate results for the fundamental frequency as well as for the overtones.

In this Note, the formula of Peters is modified, based on analogy, to include the influence of shear deformation and rotary inertia. Though the theoretical basis is not formal, comparison with exact results shows that the present expressions give surprisingly accurate results for frequencies, even for very short beams.

Approximate Expression for the Frequency

The differential equation of motion for the flapping vibrations of a rotating beam including the influence of shear deformation and rotary inertia is[4]

$$(1 + \delta\alpha p)W'''' + 3\delta\alpha pW''' - [1 - \varepsilon\delta(\lambda + \alpha)] \times (\alpha p'W' + \lambda W) + [\delta\lambda + (\varepsilon + \varepsilon\delta\alpha p)(\lambda + \alpha) - \alpha(p - 3\delta p'')]W'' = 0 \tag{1}$$

In Eq. (1), W is the total lateral displacement that is the sum of the bending and shearing displacements. The other quantities are

$$\xi = \frac{x}{L}, \quad \alpha = \frac{mL^4\Omega^2}{EI}, \quad \lambda = \frac{mL^4\omega^2}{EI}, \quad \delta = \frac{EI}{GKAL^2}$$
$$\varepsilon = \frac{I_z}{mL^2}, \quad p = \frac{1}{2}(1 - \xi^2), \quad ()' = \frac{\partial()}{\partial\xi} \tag{2}$$

where x is the axial coordinate, L is the length of the beam, m is the mass per unit length, EI is the bending rigidity, A is the area of cross section of the beam, G is the shear modulus, I_z is the mass moment of inertia in flap, and K is the Timoshenko shear coefficient that accounts for the influence of shear deformation,[5] and δ and ε are the shear deflection coefficient and rotary inertia coefficient, respectively.[4]

The equation of motion of a rotating Euler–Bernoulli beam is obtained from Eq. (1) by setting δ and ε equal to zero as

$$W'''' - \alpha(pW)' - \lambda W = 0 \tag{3}$$

For a rotating Euler–Bernoulli cantilever beam, Peters obtained an approximate formula for the nth (nondimensional) frequency as

$$\lambda_n = n(2n - 1)\alpha + \lambda^0_{NR} + F\sqrt{\alpha}\tan^{-1}\left[\frac{A_{nn} - n(2n - 1)}{F}\sqrt{a}\right] \tag{4}$$

where λ^0_{NR} = nth frequency of nonrotating beam:

$$F = \frac{\sqrt{2}}{\pi}(4n - 1)\left[\frac{(2n)!}{n!(n - 1)!_2}\frac{1}{2^{2n-1}}\right] \tag{5}$$

$$A_{nn} = \frac{1}{2}\int_0^1 (1 - \xi^2)\phi_n'^2\, d\xi \tag{6}$$

In Eq. (6), ϕ_n is the nth mode shape of a nonrotating uniform cantilever beam. Equation (4) represents an approximation valid for all stiffnesses and frequencies. The first term is the rotating string frequency (for large α or small EI). In the third term A_{nn} is the centrifugal stiffness for small α, and F is the correction to λ of the order of $(1/\sqrt{\alpha})$.

Since the equations for free vibrations in lead–lag of a Euler–Bernoulli beam can be obtained by replacing λ_n by $(\lambda_n + 1)$ (Ref. 3), Eq. (4) can be used to obtain the lead–lag frequency with λ_n replaced by $(1 + \lambda_{n\,\text{Lead-Lag}})$.

To include the influence of δ and ε in Eq. (4), the following reasoning is used:

1) The first term in Eq. (4) represents the limit when stiffness tends to zero (rotating string) and is not affected by δ and ε.

2) The second term corresponds to the nonrotating frequency of the Timoshenko beam for which exact solutions are available.

Depending on the values of δ and ε, the frequencies are lower than those of corresponding Euler–Bernoulli values. In addition, the term containing $\alpha\delta p$ in Eq. (1) tends to further reduce this frequency. Hence, the second term in Eq. (4) is proposed to be replaced by

$$[1 - (\alpha\delta/2^n)]f_1\lambda^0_{NR} \tag{7}$$

Received May 25, 1994; revision received Nov. 23, 1995; accepted for publication Dec. 29, 1995.

*Additional General Manager (Design), Helicopter Design Bureau, P.O. Box 1789.